https://doi.org/10.5194/egusphere-2024-2215
Preprint. Discussion started: 19 August 2024

Water Vapor Transport and its Influence on Water Stable Isotope in Dongting Lake Basin

Xiong Xiao[1], Xinping Zhang[1,2*], Zhuoyong Xiao[1], Zhongli Liu[1], Dizhou Wang[1], Cicheng Zhang[1], Zhiguo Rao[1], Xinguang He[1,2], Huade Guan[3]

[1] *College of Geographic Science, Hunan Normal University, Changsha 410081, China*

[2] *Key Laboratory of Geospatial Big Data Mining and Applications in Hunan Province, Hunan Normal University, Changsha 410081, China*

[3] *College of Science and Engineering, Flinders University, Adelaide SA 5001, Australia*

ABSTRACT: Understanding water vapor sources and transport paths is essential for assessing the water cycle and predicting precipitation accurately. Utilizing water vapor diagnosis and calculations, this study determined the water vapor sources and transport paths leading to precipitation in the Dongting Lake Basin in four seasons (represented by January, April, June, and October). In January, the water vapor generating precipitation originated from the Arabian Peninsula, driven by the southern branch of the westerlies over the southern side of the Tibetan Plateau, along the northern side of the Indian Peninsula through southwest China to reach the Dongting Lake Basin. In April, two transport paths emerged: one aligned closely with the January transport path but the location shifted slightly northward by one degree of latitude, and another was driven by the weak subtropical high over the southwestern Pacific, bringing moist air from the western Pacific via the South China Sea and Indochinese Peninsula. In June, the Dongting precipitation sourced from the northern branch of the South Indian Ocean

* Corresponding author. Tel.: +86-13308486020; E-mail address: zxp@hunnu.edu.cn

https://doi.org/10.5194/egusphere-2024-2215
Preprint. Discussion started: 19 August 2024

subtropical high, crossed the equator and transported through various water bodies to southwestern China, finally reaching the basin. October saw a water vapor transport path from the western Pacific, crossing the South China Sea, and entering the Dongting Lake Basin influenced by the East Asian monsoon system. In different seasons, the variations in water stable isotopes along water vapor transport paths adhered to Rayleigh fractionation and water balance principles. These findings highlight the impact of atmospheric circulation on precipitation and isotopes, providing a framework for understanding water vapor isotope mechanisms and reconstructing past atmospheric conditions.

Keywords: Dongting Lake Basin; Water vapor sources; Transport paths; Precipitation isotopes; Precipitation amount.

Significance Statement

This research explores how water vapor transports and contributes to precipitation in the Dongting Lake Basin throughout different seasons. Understanding these paths is crucial because it helps us predict and manage water resources better, which is vital for agriculture, ecosystems, and communities relying on this water. By identifying the origins and paths of water vapor, we gain insights into how global climate patterns influence local weather. This knowledge is not only critical for accurate weather forecasting but also for preparing for future climate changes. Our findings highlight the complex interactions between the atmosphere and water cycle, offering a clearer picture of how seasonal shifts in atmospheric circulation impact regional precipitation patterns.

1. Introduction

https://doi.org/10.5194/egusphere-2024-2215
Preprint. Discussion started: 19 August 2024

Diagnosing water vapor sources and analyzing water vapor transport are routine and foundational tasks, particularly within hydrometeorological services (Gimeno et al., 2020; Xu et al., 2020). A correct understanding of water vapor sources and transport is crucial for accurately evaluating the hydrological cycle and effectively predicting precipitation. For instance, in weather forecasting for the East Asian region, an essential condition for the occurrence of precipitation is the presence of sufficiently warm and moist air from low latitudes (Barker, et al., 2015; Tang et al., 2015; Hu et al., 2021). Moreover, the primary cause of meteorological drought in the East Asian monsoon region is often attributed to an anomalous decrease in water vapor sourced from the Bay of Bengal (He et al., 2022; Liu et al., 2023). Additionally, studies have shown that the abundance of stable isotopes in speleothems is related to monsoon intensity and is consequently linked to water vapor transport (Rao et al., 2013; 2016; Liang et al., 2020).

Over the past few decades, the employment of diverse mathematical models has been the crucial approach to track and deduce atmospheric water vapor sources and transport paths (Gimeno et al., 2020; Xu et al., 2020; Pranindita et al., 2022; Lekshmy et al., 2022). For instance, Pranindita et al. (2022) employed the water vapor tracking model WAM-2layers to trace back the water vapor sources during heatwaves in northern, western, and southern Europe, the reasons for the reduction of the local precipitation can be attributed to a significant reduction in water vapor supply from the North Atlantic due to anticyclonic patterns, along with the increased water vapor fluxes from eastern Eurasia and local regions. Utilizing the Lagrangian model FLEXPART v9.0, Pérez-Alarcón et al. (2023) identified precipitation water vapor sources associated

https://doi.org/10.5194/egusphere-2024-2215
Preprint. Discussion started: 19 August 2024

with the development of Indian Ocean tropical cyclones. Results showed that the water vapor sources and transport mechanisms were different during different lifecycle stages of tropical cyclones. Among numerous methods, the use of HYSPLIT for tracking water vapor sources is widespread, which employs backward trajectory calculations and atmospheric wind field information to derive water vapor transport trajectories at given heights during a precipitation event, making it commonly used for tracing water vapor during short-duration precipitation events (Draxler and Hess, 1998; Esquivel-Hernández et al., 2019; Nie and Sun, 2022; Liu et al., 2023). However, due to inherent model structure and tracking principles, derived water vapor transport paths at different heights may vary or even be opposite. Moreover, this method cannot ascertain whether the tracked water vapor indeed causes precipitation, nor can it provide information on the magnitude of water vapor transport (Wu et al., 2015; Wu et al., 2022; Deng et al., 2024).

With the continuous improvement of observational techniques and analytical methods, utilizing reanalysis data to determine the water vapor sources that cause precipitation has become a common practice (Sun et al., 2011; Hoffmann et al., 2019; Guo et al., 2019). For instance, Sun et al. (2011) investigated the climatic characteristics and decadal variations in water vapor transport in Eastern China based on NCEP/NCAR reanalysis data from 1979 to 2009. The results revealed that the variability in water vapor transport in the region is attributed to the combined influences of the Indian summer monsoon and the East Asian summer monsoon. Based on the dataset from ERA5 and isoGSM2, Xiao et al. (submitted) found a strong positive correlation

https://doi.org/10.5194/egusphere-2024-2215
Preprint. Discussion started: 19 August 2024

between seasonal precipitation and seasonal water vapor budget in the Changsha region. They noted that southwestward water vapor transport contributes significantly to water vapor input in all seasons, and only southwestward water vapor flux exhibits a highly significant positive correlation with regional precipitation amount. Although water vapor input from the northwest direction exists, there is no correlation between water vapor transport in that direction and water vapor budget or precipitation amount, while it even shows a negative correlation in some cases. Since the direction of water vapor transport has an important influence on regional precipitation, it is necessary to reveal the influences of atmospheric circulation such as the water vapor source regions and water vapor transport paths, which determine the water vapor transport direction.

Water vapor transport controlled by atmospheric circulation not only determines precipitation events but also directly influences the precipitation isotopes, thus analyzing the water vapor sources and water vapor transport paths, as well as their influences on stable isotopes under different seasons, can elucidate the mechanisms influencing the atmospheric stable isotopes (Zhou et al., 2019; Dahinden et al., 2021; Zhan et al., 2023). For instance, Risi et al. (2010) conducted an analysis of water vapor and precipitation isotopes in the Sahelian region by combining water vapor budget and water vapor transport calculations, revealing that the isotopic composition of precipitation and atmospheric water vapor in the region is controlled by the intensity of air dehydration and changes in convection. Similarly, Sengupta et al. (2006) quantified the influences of different water vapor source regions on precipitation in the northern Indian monsoon region, finding that the isotopic composition of precipitation in the

https://doi.org/10.5194/egusphere-2024-2215
Preprint. Discussion started: 19 August 2024

region is influenced by changes in water vapor source and atmospheric circulations over India. Moreover, Zhou et al. (2019) separately computed the correlations between $\delta^{18}O$ values of precipitation at different sites and found that during the prevalence of the summer monsoon (April to September) and winter monsoon (October to March), the key upstream regions influencing the precipitation isotopes in the Dongting Lake Basin located in south-central China are the Bay of Bengal and southwestern China, respectively. However, as the critical regions influencing regional precipitation isotopes may not necessarily be the water vapor source regions, these studies are yet to definitively determine the water vapor source regions and water vapor transport paths.

Existing studies indicate that in the East Asian monsoon region, including the Dongting Lake Basin, differences in the water vapor sources and transport direction during different seasons are the primary drivers of seasonal variations in precipitation isotopes (Araguás-Araguás et al., 1998; Zhang et al., 2016; Wei et al., 2018; Chiang et al., 2020). Typically, during the summer monsoon, prevailing southeast or southwest winds dominate the East Asian monsoon region, with water vapor for precipitation originating from low-latitude oceans (Barker, et al., 2015; Wu et al., 2015; Tang et al., 2015), while precipitation isotopes are significantly depleted influenced by intense rainout effects along the water vapor transport paths during this period (Zhou et al., 2019; Wu et al., 2022). Conversely, during the winter monsoon, northwest or northeast winds prevail in the East Asian monsoon region, by simple deduction, the precipitation isotopes should be more enriched if water vapor for precipitation is carried by westerlies or originates from the evaporation of inland regions (e.g., Liu et al., 2011; Wu et al.,

https://doi.org/10.5194/egusphere-2024-2215
Preprint. Discussion started: 19 August 2024

2015; Shi et al., 2021). However, both actual observations from the Global Network of Isotopes in Precipitation (GNIP) and simulations from isotope-enabled General Circulation Models (isoGCMs) consistently demonstrate that, whether during the summer or winter monsoon, the spatial distribution of precipitation isotopes in the East Asian monsoon region exhibits significant latitudinal and continental effects—that is, the precipitation isotopes become more depleted with the increases of latitude or distance from the ocean (Feng et al., 2009; Zhang et al., 2012; Zhang et al., 2016). Consequently, the observed water vapor transport during the summer monsoon aligns with the spatial distribution of precipitation isotopes under the influence of latitudinal and continental effects and is consistent with the Rayleigh distillation principle for water stable isotopes, however, water vapor transport during the winter monsoon does not follow the above spatial distribution and Rayleigh distillation principle (Tang et al., 2015; Zhou et al., 2019; Wu et al., 2022).

Based on the understanding outlined above, a thorough investigation into the seasonal variations in water vapor sources and transport paths for precipitation amount and isotopes in the East Asian monsoon region is necessary, which may provide significant benefit for accurately understanding regional hydrological mechanisms and elucidating regional climate characteristics. Focusing on the Dongting Lake Basin within the East Asian monsoon area, and drawing upon fundamental theories of meteorology, water vapor diagnostics, and water vapor calculations, this study aims to (1) identify the water vapor sources and transport paths contributing to the Dongting Lake Basin; (2) analyze the variations in meteorological factors and water stable

https://doi.org/10.5194/egusphere-2024-2215
Preprint. Discussion started: 19 August 2024

isotopes along the water vapor transport paths; and (3) reveal the mechanisms by which water vapor sources and transport paths in the monsoon region influencing precipitation amounts and isotopes.

2. Methods and materials

2.1 Study site

Dongting Lake Basin, situated in the south-central region of China (Fig. 1), is a basin characterized by a subtropical monsoon climate, marked by distinct four seasons and moderate humidity. Winters are moist and cold, while summers are warm and moist. Based on historical meteorological data from 1960 to 2017, the Dongting Lake Basin experiences an average annual precipitation of 1375.6.0 mm. During the colder months (October to March of the following year), precipitation is relatively low due to the influence of continental air masses. However, from late April onward, influenced by maritime monsoons, precipitation increases significantly, accompanied by a notable rise in temperature, with precipitation predominantly occurring from April to June (Liu et al., 2023; Xiao et al., 2024).

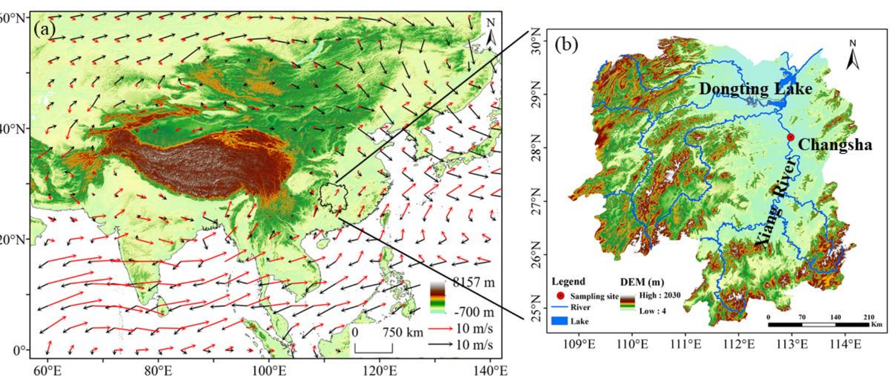

Fig. 1 Map showing the location of the Dongting Lake Basin, and the Changsha

https://doi.org/10.5194/egusphere-2024-2215
Preprint. Discussion started: 19 August 2024

sampling site in the East Asian Monsoon Region. Note that the black arrow and red arrow in subplot (a) represent the average wind field at 850 hPa in January and June, respectively.

The prevailing wind refers to the wind or wind direction that appears the most frequently in a region during a specific period. Its occurrence is closely related to the atmospheric circulation of the region. In the East Asian monsoon region, which includes the Dongting Lake Basin, the strong cold high-pressure system influences the winter season, resulting in prevailing northerly winds near the surface, with northwesterly winds prevailing in the basin as shown by the average wind field at the 850 hPa in January, i.e. the black arrow in Fig. 1a. In the summer, influenced by the Western Pacific Subtropical High and the Indian Low, the near-surface winds are predominantly southerly in the East Asian monsoon region, with southwesterly winds prevailing in the Dongting Lake Basin as shown by the average wind field at the 850 hPa in June, i.e. the red arrow in Fig. 1a. Positioned at the convergence of the prevailing northerly winds, prevailing southerly winds, and westerly winds, the Dongting Lake Basin experiences complex precipitation processes and different precipitation amounts in different seasons and water vapor transport directions. This complexity results in high variability in the precipitation isotope dynamics (Zhou et al., 2019; Xiao et al., 2024).

2.2 Water samples collection and analysis

From January 1, 2010 to December 31, 2022, precipitation sample sampling has been conducted at the Meteorological Garden of Hunan Normal University in Changsha (28°11’N, 112°56’E). The sampling protocol followed the meteorological observation

https://doi.org/10.5194/egusphere-2024-2215
Preprint. Discussion started: 19 August 2024

standards of China's meteorological departments, with samples collected at 08:00 and 20:00 Beijing time on precipitation days. Liquid precipitation was directly collected in sealed 30 ml polyethylene bottles after measuring the precipitation amount, while solid precipitation was first collected in air-tight plastic bags, then measured for meltwater volume after natural melting, and transferred to the same size polyethylene bottles. All the collected water samples were stored in a refrigerator at 0°C before testing.

Precipitation sample analysis from 2010 to 2013 was conducted using a Liquid Water Isotope Analyzer (DLT-100, Model: 908-0008) from Los Gatos Research, USA; subsequently, a new generation Liquid and Gas Dual-Mode Stable Isotope Analyzer (IWA-35EP, Model: 912-0026-1000) from the same company was used from 2014 to 2022. The oxygen and hydrogen stable isotope ratio in the water samples were expressed in per mil (‰) deviations relative to the Vienna Standard Mean Ocean Water (V-SMOW), calculated using the equation:

$$\delta^{2}\mathrm{H} \text{ or } \delta^{18}\mathrm{O} = \left[{R_{s}}/{R_{\text{V-SMOW}}} - 1 \right] \times 1000 \quad (1)$$

In the equation, R_s and $R_{\text{V-SMOW}}$ represent the oxygen (or hydrogen) stable isotope ratios $^{18}O/^{16}O$ (or $^{2}H/^{1}H$) in the water sample and in Vienna Standard Mean Ocean Water (V-SMOW), respectively. The testing precision averaged $\delta^{18}O \leq 0.3‰$ and $\delta^{2}H \leq 2‰$ during 2010-2013, and $\delta^{18}O \leq 0.2‰$ and $\delta^{2}H \leq 0.6‰$ during 2014-2022. If there were two precipitation samples in one day, the precipitation stable isotope values for that day were represented by the volume-weighted average. In total, 1668 precipitation days' $\delta^{18}O$ ($\delta^{2}H$) data were obtained over the past 13 years.

2.3 Ancillary data

https://doi.org/10.5194/egusphere-2024-2215
Preprint. Discussion started: 19 August 2024

ERA5, produced and released by the European Centre for Medium-Range Weather Forecasts (ECMWF), is the fifth-generation global atmospheric reanalysis data product from the center. Compared to its predecessor ERA-Interim, ERA5 incorporates a state-of-the-art integrated forecasting system, integrates more historical observational data, and reprocesses a large amount of assimilation data, resulting in significantly improved accuracy (Albergel et al., 2018; Hoffmann et al., 2019). Additionally, ERA5 features substantial improvements in temporal and spatial resolution. The temporal resolution has increased from 6 hours in ERA-Interim to 1 hour, while the horizontal resolution has improved from 79 km to 31 km, and the highest vertical extension reaches 0.01 hPa altitude. These enhancements enable ERA5 to capture finer atmospheric details. Moreover, the number of variables provided by ERA5 has increased from over 100 in ERA-Interim to the current 240, and the data release delay has been reduced from 2-3 months in ERA-Interim to 5 days (Albergel et al., 2018; Hoffmann et al., 2019). The reanalysis data used in this study include surface pressure, specific humidity at 1000/850/700/600/500/400/300 hPa, altitudinal wind, and meridional wind. The horizontal resolution is 1°×1°, with a temporal step of 1 hour. This dataset was used to calculate the vertical integral of water vapor fluxes into a specified region, introduced in section 2.4.

Since the fractionation process of water stable isotopes in the atmosphere cannot be directly observed, analyzing the variations of atmospheric stable isotopes requires the application of stable isotopes fractionation theory along with the fundamental principles and methods of meteorology. In terms of research methods, the introduction

https://doi.org/10.5194/egusphere-2024-2215
Preprint. Discussion started: 19 August 2024

of atmospheric circulation models for water stable isotope cycling, such as isoGCMs, provides a unique and effective tool. Among numerous isoGCMs, isoGSM (Isotope-incorporated Global Spectral Model) exhibits relatively good simulation performance in the East Asian region (Zhang et al., 2020; Kathayat et al., 2021). isoGSM is a stable isotope GCM developed by Yoshimura et al. (2008), which integrated water isotope cycling and fractionation processes into the Global Spectral Model at the Scripps Experimental Climate Prediction Center. The driving factors include sea surface temperature, sea ice, and temperature and horizontal wind fields in 28 vertical layers. This model addresses the Gibbs phenomenon in atmospheric circulation models and performs better in simulating water vapor transport processes in arid and high-altitude regions (Yoshimura et al. 2008; Bong et al., 2024). The second-generation isoGSM2 has a higher temporal and spatial resolution in simulating water vapor and precipitation isotopes compared to the first-generation (Chiang et al., 2020). It utilizes the NECP-R2 (National Centers for Environmental Prediction Reanalysis 2) reanalysis dataset and abandons the NDSL (Non-iteration Dimensional-split Semi-Lagrangian) advection scheme used in the previous generation. By dynamically correcting the model output using reanalysis data, isoGSM2's simulation results are closer to actual atmospheric conditions, thereby improving the accuracy of water vapor and precipitation isotope simulations (Bong et al., 2024).

The water stable isotope simulation data used in this study are from isoGSM2 (January 1979 to December 2017, totaling 468 months), including monthly precipitation amount (*P*), stable isotopes (δ^2H and δ^{18}O) in the precipitation and vertical

https://doi.org/10.5194/egusphere-2024-2215
Preprint. Discussion started: 19 August 2024

integral of water vapor (δ^2H_v, $\delta^{18}O_v$, δ^2H_p, and $\delta^{18}O_p$), and the calculated deuterium excess in water vapor and in precipitation (Ex_d_v and Ex_d_p). The spatial scale ranges from 30°S to 70°N and 0° to 280°E, with a horizontal resolution of 1°×1° (Chiang et al., 2020; Liu et al., 2023).

2.4 Model Analysis

The water vapor transport flux serves as a metric for both the magnitude and direction of water vapor transport, representing the mass of water vapor passing through a unit cross-section per unit of time (Sun et al., 2011). The specific calculation equation is as follows:

$$Q = \frac{1}{g}\int_{p_t}^{p_s} Vq\mathrm{d}p \qquad (2)$$

Where the meridional component Q_λ and the latitudinal component Q_φ of the water vapor transport flux are given by:

$$Q_\lambda = \frac{1}{\mathrm{g}}\int_{p_t}^{p_s} uq\mathrm{d}p \qquad (3)$$

$$Q_\varphi = \frac{1}{\mathrm{g}}\int_{p_t}^{p_s} vq\mathrm{d}p \qquad (4)$$

Here, Q represents the vertical integral of water vapor flux ($\mathrm{kg \cdot m^{-1} \cdot s^{-1}}$), including the meridional component Q_λ and the latitudinal component Q_φ. V denotes the vector wind speed ($\mathrm{m \cdot s^{-1}}$), including the latitudinal wind speed (v) and meridional wind (u), q represents specific humidity ($\mathrm{kg \cdot kg^{-1}}$), g is the acceleration due to gravity ($\mathrm{m \cdot s^{-2}}$), p_s is the lower boundary pressure (hPa), and p_t is the upper boundary pressure (hPa). In the actual atmosphere, water vapor content above 300 hPa is minimal, thus p_t is set to 300 hPa when calculating the vertical integral of water vapor flux through the entire

https://doi.org/10.5194/egusphere-2024-2215
Preprint. Discussion started: 19 August 2024

atmospheric column.

3. Results

3.1 Seasonal Variation Characteristics of Precipitation Isotopes in the Changsha Region

The monthly weighted average and total monthly calculations were performed on the daily $\delta^{18}O_p$, daily Ex_d_p, and daily *P* collected from the Hunan Normal University and the Changsha National Meteorological Reference Station, yielding the seasonal variations of multi-year monthly weighted average $\delta^{18}O_p$, monthly weighted average Ex_d_p, and monthly average *P* in the Changsha region (Fig. 2a). The $\delta^{18}O_p$, Ex_d_p, and *P* in Changsha exhibited significant seasonal variations—that is, the maximum value of $\delta^{18}O_p$ appeared in March and April, both at −3.57‰, but did not correspond to the months with the lowest precipitation amounts. The three lowest values of $\delta^{18}O_p$ occurred in July, August, and September, respectively at −9.45‰, −8.93‰, and −9.42‰, with a simple arithmetic average of −9.27‰, which also did not correspond to the months with the highest precipitation amounts. The maximum value of Ex_d_p (20.05‰) appeared in January, and the minimum value (9.29‰) appeared in August, both of which were months with relatively low precipitation. Due to these significant differences in the phases of precipitation isotopes and amounts, it is apparent that explaining the variations in local precipitation stable isotopes solely based on the seasonal variations in local precipitation amounts is insufficient.

https://doi.org/10.5194/egusphere-2024-2215
Preprint. Discussion started: 19 August 2024

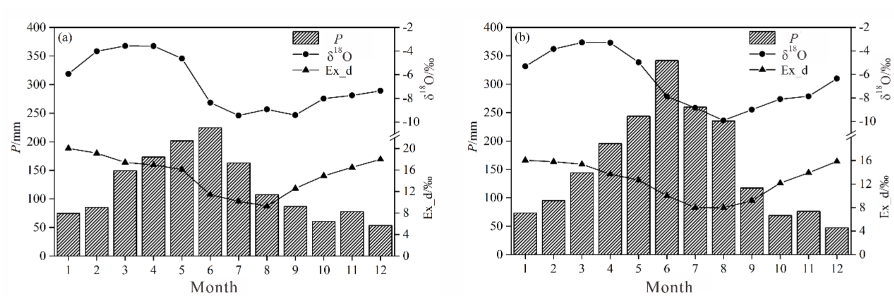

Fig. 2 Comparisons between seasonal variations of precipitation $\delta^{18}O$ ($\delta^{18}O_p$), precipitation excess deuterium (Ex_d_p), and precipitation amount (*P*) measured at the Changsha station (a) and simulated by isoGSM2 or driven from the RA5 reanalysis dataset at the corresponding grid (b).

Monthly weighted average calculation was performed on the monthly $\delta^{18}O_p$ and Ex_d_p simulated by isoGSM2 at the Changsha grid, and the monthly average calculation was performed on the *P* from ERA5, yielding the seasonal variations of simulated monthly weighted average $\delta^{18}O_p$ and Ex_d_p and ERA5 monthly average *P* at the Changsha grid (Fig. 2b). The simulated and calculated $\delta^{18}O_p$, Ex_d_p, and *P* in Changsha all effectively reproduced the seasonal variations of the corresponding observations. The root mean square errors (RMSE) between simulated and observed values were 0.54‰, 2.78‰, and 59.7 mm, respectively. Corresponding to the observed seasonal variations, the two maximum values of the simulated $\delta^{18}O_p$ occurred in March and April, at −3.29‰ and −3.31‰, respectively, with very small differences from the observed values. The three lowest values of simulated $\delta^{18}O_p$ also occurred in July, August, and September, at −8.84‰, −9.92‰, and −9.00‰, respectively, with a simple arithmetic average of −9.25‰, which was consistent with the observed values. The maximum value of simulated Ex_d_p (16.05‰) appeared in January, and the minimum

https://doi.org/10.5194/egusphere-2024-2215
Preprint. Discussion started: 19 August 2024

value (7.97‰) appeared in August (Fig. 2b), both consistent with the observed values (Fig. 2a). These comparisons indicated that isoGSM2 exhibited strong capabilities in simulating the spatial distribution and temporal variations of atmospheric water stable isotopes.

To analyze the seasonal variation in the atmospheric water vapor transport and its influences on the regional precipitation isotopes, and taking into account the hydro-climatic characteristics of the study region (Fig. 2), four representative months including January, April, June, and October were selected as the study seasons. Among these representative months, January in the Changsha region represents winter, characterized by the lowest temperatures and relatively low precipitation throughout the year. April signifies spring, with rapidly increasing precipitation amounts and frequent fluctuations between warm and cold air masses. June represents the peak of the summer monsoon season, with the highest monthly precipitation amount of the year. October represents autumn, characterized by clear and cool weather and the second-lowest precipitation throughout the year under the influence of the West Pacific Subtropical High.

3.2 Water Vapor Transport in the Dongting Lake Basin in Different Seasons

3.2.1 Average Water Vapor Transport Path in the Dongting Lake Basin in January

Based on the ERA5 reanalysis data, we calculated and plotted the spatial distribution of the 500 hPa average geopotential height (H_{500}) and average Q (Fig. 3a), multi-year average P (Fig. 3b) in January. Moreover, based on the isoGSM2 simulation data, we plotted the spatial distributions of the average $\delta^{18}O_v$ (Fig. 3c), $\delta^{18}O_p$ (Fig. 3d),

https://doi.org/10.5194/egusphere-2024-2215
Preprint. Discussion started: 19 August 2024

Ex_d$_v$ (Fig. 3e), and Ex_d$_p$ (Fig. 3f) in January.

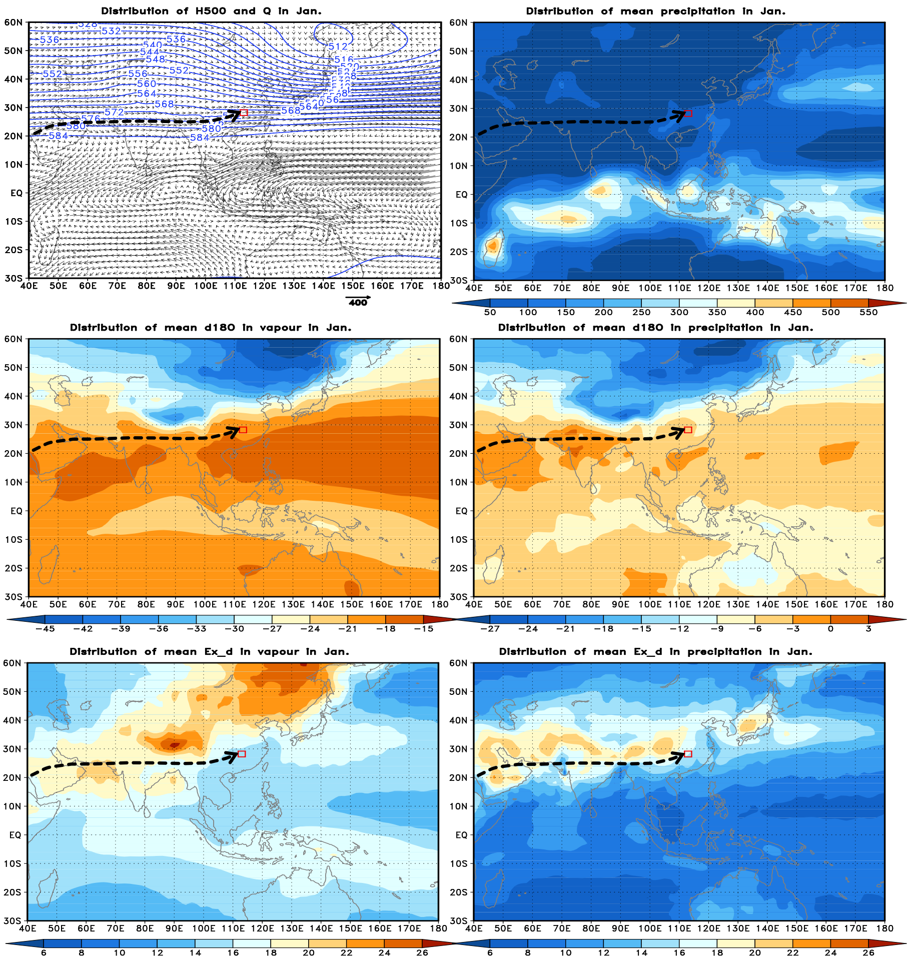

Fig. 3 Mean vapor transport path to the Dongting Lake Basin and the spatial distributions of Q with H_{500} (a), P (b), $\delta^{18}O_v$ (c), $\delta^{18}O_p$ (d), Ex_d$_v$ (e), and Ex_d$_p$ (f) in January. Q, H_{500}, P, $\delta^{18}O_v$, $\delta^{18}O_p$, Ex_d$_v$, and Ex_d$_p$ represent the vertical integral of water vapor flux, 500 hPa average geopotential height, precipitation amount, $\delta^{18}O$ in atmospheric water vapor and precipitation, and deuterium excess in atmospheric water vapor and precipitation, respectively, hereinafter the same.

At the H_{500} field of East Asia, the deep East Asian Trough was stably located along

https://doi.org/10.5194/egusphere-2024-2215
Preprint. Discussion started: 19 August 2024

the East coast, and the strong Ural Ridge in the mid-high latitudes of 70°E to 90°E (Fig. 3a). Influenced by the northwest airflow behind the trough and ahead of the ridge, the northwest winds prevailed in most parts of East Asia. In the Dongting Lake Basin (highlighted in the red box in Fig. 3), influenced by the middle-latitude westerly belt, water vapor transport mainly was from west to east. Under the control of the cold continental high, precipitation was relatively low over the entire East Asia and South Asia, while the regions with high *P* values were mainly distributed in the equatorial convergence zone and the North Pacific located ahead of the East Asian Trough (Fig. 3b). Unlike most regions of the East Asian continent, the Dongting Lake Basin lied on a wet tongue, benefiting from the Southwest Vortex in the eastern Tibetan Plateau (Lai et al., 2023; Huang and Li, 2023).

The $\delta^{18}O_v$ and $\delta^{18}O_p$ in January exhibited significant continental effects (Figs. 3c and 3d). Under the control of continental cold air masses, the centers of minimum $\delta^{18}O_v$ and $\delta^{18}O_p$ values were located in the mid-high latitudes of Eastern Siberia. Due to the influence of topography, the $\delta^{18}O_v$ tended to be negative over the Tibetan Plateau. These two low-value regions correspond to the cold pole of Eurasia and the Earth's third pole, respectively. Regions enriched in atmospheric water isotopes were mainly distributed over vast oceans and Western Asia. In the equatorial convergence zone, due to the rainout effects, both water vapor isotopes and precipitation isotopes were depleted to some extent. Along with the surrounding the Dongting Lake Basin, the abundance of water vapor isotopes and precipitation isotopes in the Dongting Lake Basin were comparable to those of the middle-low latitude oceans in January.

The spatial distributions of the Ex_d_v and Ex_d_p exhibited the characteristics of low in the ocean and high in the land, but the regions where their maximum values occurred did not completely correspond (Figs. 3e and 3f). The maximum value of the Ex_d_v mainly appeared in Eastern Siberia and the Tibetan Plateau, showing a meridional distribution from northeast to southwest, while the high values of the Ex_d_p mainly occurred in mid-latitude inland regions, showing a latitudinal distribution from west to east. The Ex_d_v and Ex_d_p values in the Dongting Lake Basin lay exactly in the transition region from low to high values. Typically, the Ex_d_p largely depended on the Ex_d_v, but processes such as condensation in clouds, secondary evaporation below clouds, evaporation from underlying surfaces, and the exchange and diffusion of water vapor isotopes could cause precipitation isotopes to deviate to varying degrees from atmospheric water vapor isotopes (Zhang et al., 2016).

In the Q field (Fig. 3a), a vector interpolation method was applied regarding the Changsha site as the endpoint, as well as based on the drawing of streamlines, the average water vapor transport path in January was obtained (black arrow lines in Fig. 3). This transport path originated near the Arabian Peninsula. Driven by the southern branch of the westerly stream jet on the southern side of the Tibetan Plateau, water vapor transported along the southern side of the Tibetan Plateau, passed through southwestern China via the northern part of the Indian Peninsula, and reached the Dongting Lake Basin. It can be seen that this water vapor transport path was not consistent with the prevailing wind direction in January as shown in Fig. 1a. Six series of factors at the grid points along the water vapor transport path were derived from each

https://doi.org/10.5194/egusphere-2024-2215
Preprint. Discussion started: 19 August 2024

factor field in January, including the variations of Q, P, $\delta^{18}O_v$, $\delta^{18}O_p$, Ex_d_v, and Ex_d_p. As shown in Fig. 4, both the Q and P were relatively low, while increased to some extent due to the converging effect of Southwest Vortex after entering the Dongting Lake Basin (Figs. 4a and 4b). Under the weak atmospheric meridional disturbances in January, the changes in $\delta^{18}O_v$ and Ex_d_v were minor, fluctuating slightly around −19.06‰ and 18.16‰, respectively (Figs. 4c and 4e). Due to the low precipitation amount, the $\delta^{18}O_p$ values were relatively positive in the first half of the water vapor transport path, and then became more negative in the latter half with the enhanced rainout effect, while the Ex_d_p became more positive (Figs. 4d and 4f).

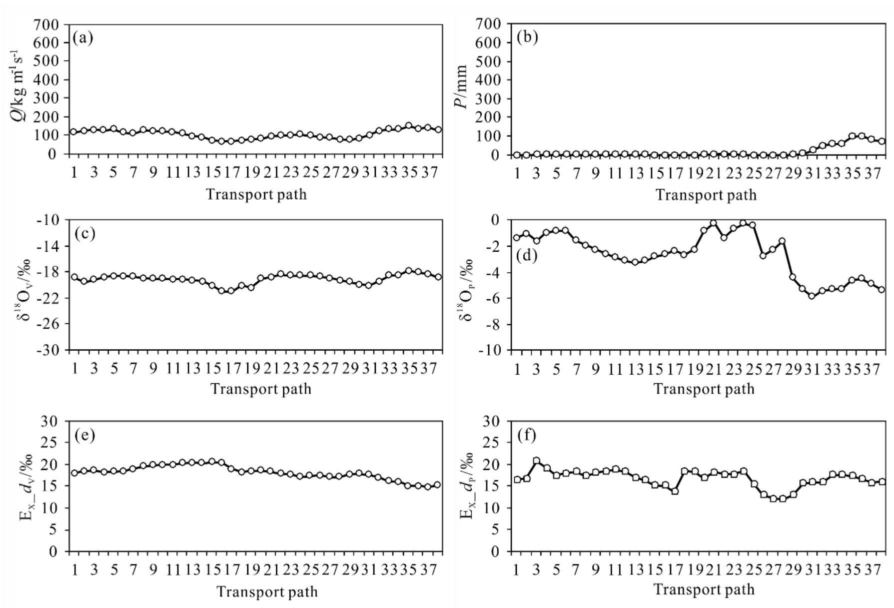

Fig. 4 Mean variations of Q (a), P (b), $\delta^{18}O_v$ (c), $\delta^{18}O_p$ (d), Ex_d_v (e), and Ex_d_p (f) along the vapor transport path in January

3.2.2 Average Water Vapor Transport Path in the Dongting Lake Basin in April

Based on the ERA5 reanalysis data and the isoGSM2 simulation data, the spatial

https://doi.org/10.5194/egusphere-2024-2215
Preprint. Discussion started: 19 August 2024

distributions of H_{500}, Q, P, $\delta^{18}O_v$, $\delta^{18}O_p$, Ex_d_v, and Ex_d_p were calculated and plotted in April (Fig. 5). At the H_{500} field (Fig. 5a), the East Asian Trough and Ural Ridge were still present in the mid-to-high latitudes. The East Asian mid-to-high latitude regions were still influenced by the winter monsoon, while its intensity was significantly weakened. In the mid-to-low latitudes, the Western Pacific subtropical high has strengthened and expanded northward, with the ridge line located approximately near 15°N. A shallow trough appeared in the northern part of the Bay of Bengal, indicating the beginning of tropical systems influencing the mid-to-low latitude regions of East Asia. In the Dongting Lake Basin, influenced by the westerlies and low-latitude atmospheric systems, the water vapor transport shifted to the domination by the southwestward direction. Most continental regions of East Asia and South Asia experienced a certain degree of precipitation increase, with the rainy band caused by the intertropical convergence zone, previously located in the Southern Hemisphere, moving to the Northern Hemisphere (Fig. 5b). The Dongting Lake Basin also entered the spring flood season in April, while the Changsha region was situated in a center with an above-average spring precipitation amount compared to the surrounding regions in this period (Fig. 5b).

https://doi.org/10.5194/egusphere-2024-2215
Preprint. Discussion started: 19 August 2024

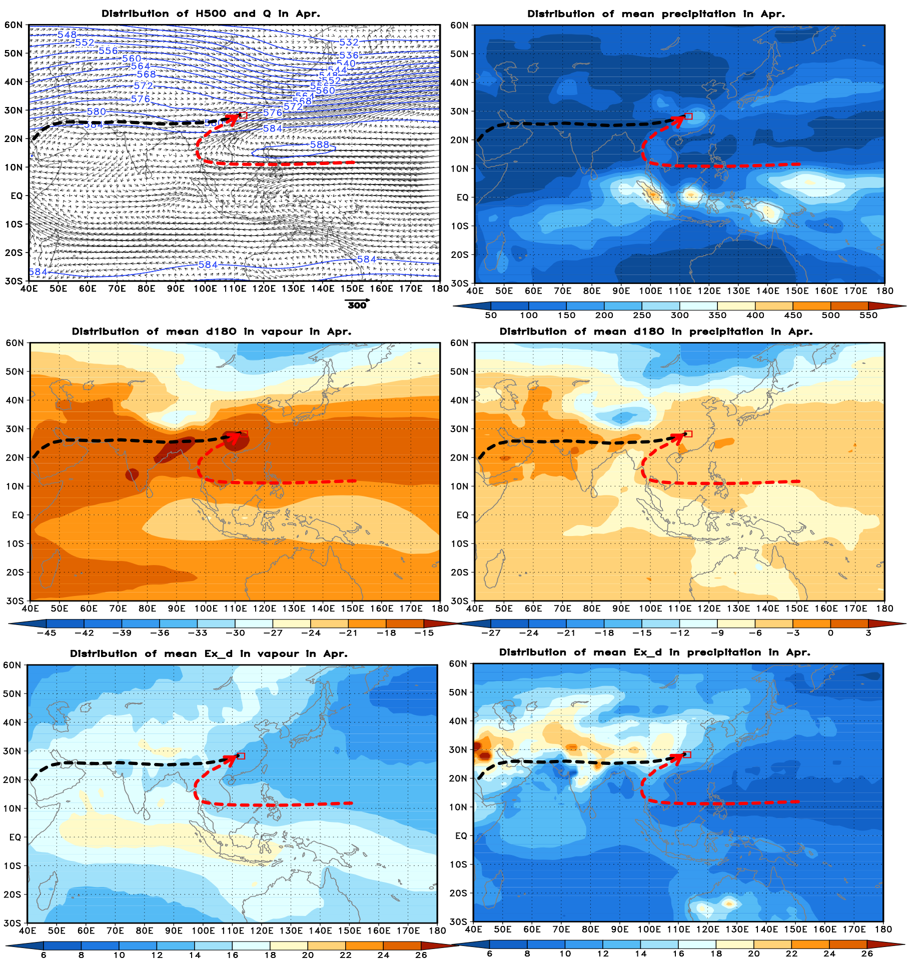

Fig. 5 Mean vapor transport paths to the Dongting Lake Basin and the spatial distributions of Q with H_{500} (a), P (b), $\delta^{18}O_v$ (c), $\delta^{18}O_p$ (d), Ex_d$_v$ (e), and Ex_d$_p$ (f) in April.

Compared to the situations in January, there were no major changes in the spatial distributions of $\delta^{18}O_v$ and $\delta^{18}O_p$ in April (Figs. 5c and 5d). In the regions with low $\delta^{18}O_v$ and $\delta^{18}O_p$ values, previously located in Eastern Siberia and the Tibetan Plateau, atmospheric stable isotopes have significantly enriched. Due to temperature rise and enhanced evaporation, the regions with high levels of $\delta^{18}O_v$ and $\delta^{18}O_p$ in the mid-to-

https://doi.org/10.5194/egusphere-2024-2215
Preprint. Discussion started: 19 August 2024

low latitudes showed continual increases in the $\delta^{18}O_v$ and $\delta^{18}O_p$ values. With the strengthening of water vapor convergence in the Dongting Lake Basin, the $\delta^{18}O_v$ in the Dongting Lake Basin showed significant increases in April, leading to an isotopic enrichment in precipitation. Compared to the large-scale region, the water isotope composition in the Dongting Lake Basin, was not significantly different from that of the mid-to-low latitude ocean, indicating the controls by the maritime air masses (Figs. 5c and 5d).

In April, the spatial distributions of Ex_d_v and Ex_d_p were comparable to the situations in January (Figs. 5e and 5f). The regions with high-value Ex_d_v, previously located in Eastern Siberia and the Tibetan Plateau, respectively, showed significant reductions in range and intensity, but the regions with low-value Ex_d_v in the Western Pacific expanded, thereby reducing the differences between land and sea. With the continuous inland influx of maritime water vapor from the Western Pacific Ocean, the range of low-value regions of the Ex_d_p has expanded. Influencing by the increasing precipitation, the range of high-value regions of the Ex_d_p in mid-latitude inland regions has narrowed, but the intensity has increased to varying degrees, especially in West Asia. Finally, both the Ex_d_v and Ex_d_p in the Dongting Lake Basin showed decreases, which were influenced by the gradually strengthening summer monsoon and the situation of water vapor transport (Figs. 5e and 5f).

Based on the vector interpolation method, two water vapor transport paths were obtained regarding the Changsha site as the endpoint (Fig. 5a). The first water vapor transport path—that is, the Path I (represented by black arrow lines in Fig. 5), was

https://doi.org/10.5194/egusphere-2024-2215
Preprint. Discussion started: 19 August 2024

essentially consistent with the water vapor transport path in January, but it is slightly shifted northward by one degree of latitude. The second water vapor transport path—that is, Path II (represented by red arrow lines in Fig. 5), driven by the weak Western Pacific subtropical high, guided warm and moist water vapor from the low latitudes of the Western Pacific along the outer edge of the subtropical high, passing through the South China Sea and the Indochinese Peninsula and finally reached into the Dongting Lake Basin. Corresponding data at the grid points along two water vapor transport paths were extracted and plotted for the Q, P, $\delta^{18}O_v$, $\delta^{18}O_p$, Ex_d_v, and Ex_d_p (Fig. 6).

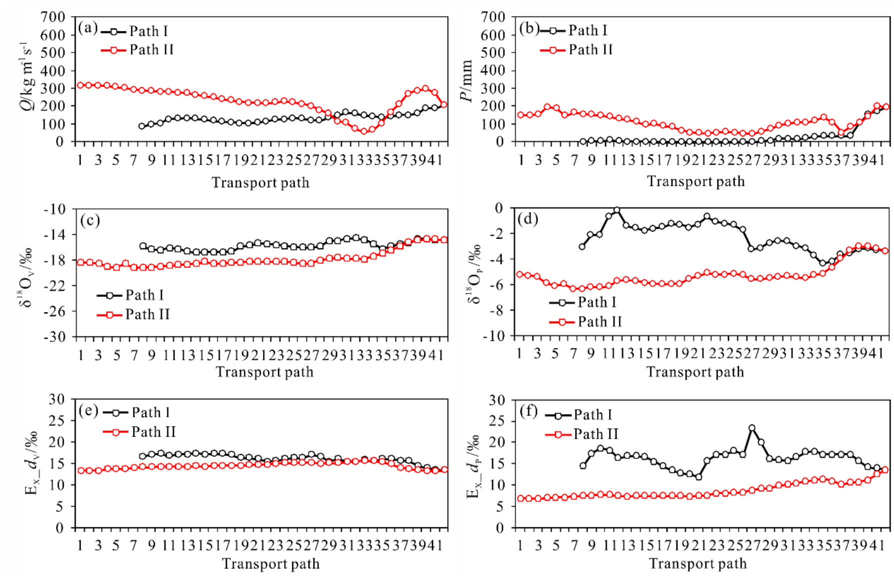

Fig. 6 Mean variations of Q (a), P (b), $\delta^{18}O_v$ (c), $\delta^{18}O_p$ (d), Ex_d_v (e), and Ex_d_p (f) along the vapor transport paths in April.

Along Path I, both the Q and P showed slight increases compared to the situations in January (Figs. 6a and 6b), with the average values in the first half of the water vapor transport path before entering the Dongting Lake Basin were 128.23 kg m^{-1} s^{-1} and 10.5

https://doi.org/10.5194/egusphere-2024-2215
Preprint. Discussion started: 19 August 2024

mm, respectively, still at relatively low levels. After entering the Dongting Lake Basin, the average Q and P increased to 180.13 kg m^{-1} s^{-1} and 135.0 mm, respectively. Under the transport of latitudinal water vapor, the $\delta^{18}O_v$ increased slightly from −15.83‰ to −14.85‰, while the $\delta^{18}O_p$ decreased slightly from −2.06‰ to −3.28‰ (Figs. 6c and 6d). The corresponding Ex_d_v decreased from 16.45‰ to 14.26‰, and the Ex_d_p decreased from 16.60‰ to 14.97‰, indicating the input of oceanic water vapor (Figs. 6e and 6f).

Along Path II, both the Q and P were significantly larger than those along the latitudinal Path I (Figs. 6a and 6b), with the average values before entering the Dongting Lake Basin were 226.6 kg m^{-1} s^{-1} and 108.2 mm, respectively. After entering the Dongting Lake Basin, these values increased to 269.2 kg m^{-1} s^{-1} and 148.6 mm, respectively. The area where Q decreased significantly corresponds to a water vapor divergence region at the southwest corner of the Indochinese Peninsula. Under the meridional water vapor transport, the $\delta^{18}O_v$ increased from −18.21‰ to −14.86‰, while the $\delta^{18}O_p$ from −5.50‰ to −3.15‰ (Figs. 6c and 6d); correspondingly, the Ex_d_v decreased from 14.61‰ to 13.50‰, while the Ex_d_p increased from 8.32‰ to 11.81‰ (Figs. 6e and 6f), following the variation rule of excess deuterium during water vapor transport (Vasil'chuk, 2014).

3.2.3 Average Water Vapor Transport Path in the Dongting Lake Basin in June

Based on the ERA5 reanalysis data and isoGSM2 simulation data, the spatial distributions of the average H_{500}, Q, P, $\delta^{18}O_v$, $\delta^{18}O_p$, Ex_d_v, and Ex_d_p were respectively calculated and plotted in June (Fig. 7). At the H_{500} field (Fig. 7a), the East

https://doi.org/10.5194/egusphere-2024-2215
Preprint. Discussion started: 19 August 2024

Asian Trough continues to stably exist in June, but the position of trough line shifted eastward over the North Pacific Ocean. The high-pressure ridge in the eastern part of the Ural Mountains weakened and shifted eastward over Lake Baikal. The rapidly intensifying western Pacific subtropical high expanded westward and northward, with its ridge line located at approximately 22~23°N, while the India-Burma Trough in the northern Bay of Bengal strengthened continuously. The atmospheric circulation situation indicated that most of East Asia, including the south of the Yangtze River, has entered the prevailing period of summer monsoon (Fig. 7a). The warm and moist water vapor from the Arabian Sea and the Bay of Bengal driven by the India-Burma Trough as well as along the outer edge of the subtropical high from the western Pacific met the cold air moving southward behind the East Asian Trough and thus generated an extremely long rain belt spanning 20 degrees of latitude and 70 degrees of longitude from India, through the Indochinese Peninsula, to southern China until central Japan (Fig. 7b). In this rain belt, the three largest precipitation centers were located on the west coast of India, the Thai-Myanmar border region, and the Jiangnan region of China. The formation of the first two precipitation centers was related to terrain, while the formation of the precipitation center in the Jiangnan region of China was related to the convergence of warm and moist water vapor from low latitudes to this region (Fig. 7b).

https://doi.org/10.5194/egusphere-2024-2215
Preprint. Discussion started: 19 August 2024

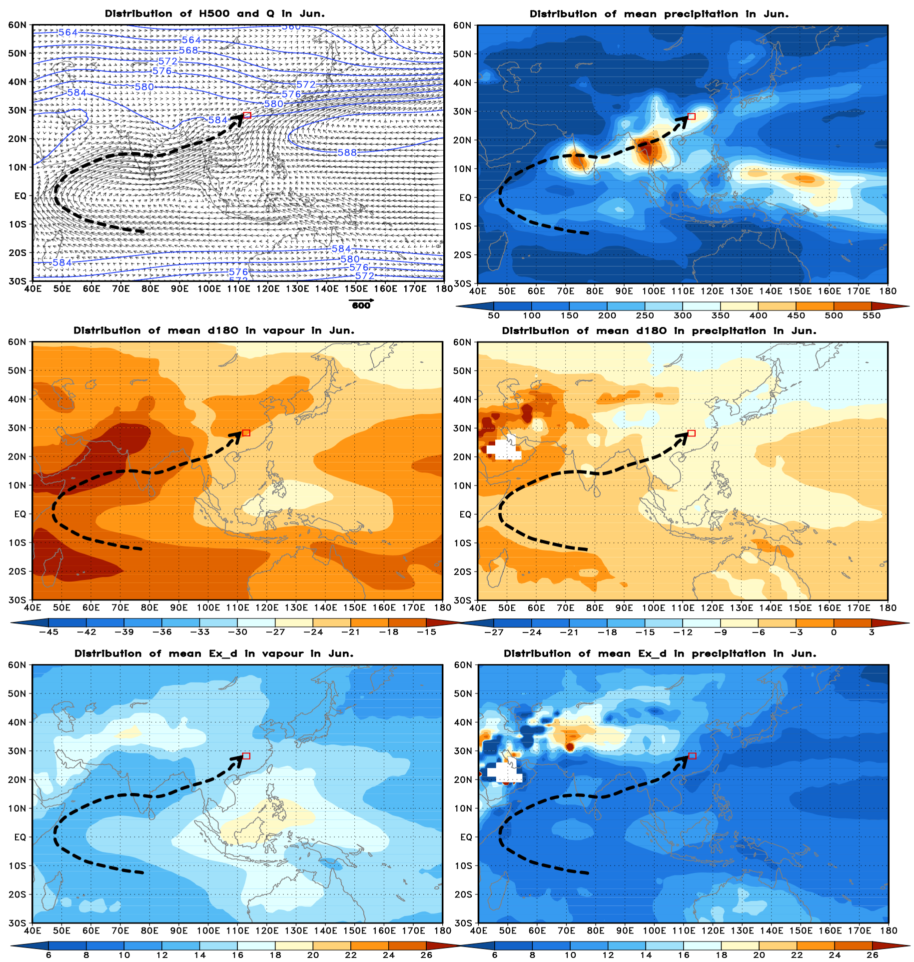

Fig. 7 Mean vapor transport path to the Dongting Lake Basin and the spatial distributions of Q with H_{500} (a), P (b), $\delta^{18}O_v$ (c), $\delta^{18}O_p$ (d), Ex_d_v (e), and Ex_d_p (f) in June.

With the change in circulation situation, the distributions of the $\delta^{18}O_v$ and $\delta^{18}O_p$ in June changed accordingly (Figs. 7c and 7d). The stable isotopes in both water vapor and precipitation at mid-high latitudes were significantly enriched, with reduced spatial differences. The $\delta^{18}O_v$ and $\delta^{18}O_p$ values remained high in the Arabian Sea, the Bay of Bengal, and the Southern Ocean, the region with high $\delta^{18}O$ in the western Pacific

https://doi.org/10.5194/egusphere-2024-2215
Preprint. Discussion started: 19 August 2024

became narrowed, and the low $\delta^{18}O$ values in the Indonesia-Philippines region in the western equatorial Pacific were associated with the enhanced water vapor convergence (Figs. 7a, 7c, and 7d). The regional low $\delta^{18}O$ center previously present in the cold season over the Tibetan Plateau had disappeared. In the Jiangnan region of China, the convergence of water vapor from low-latitude oceans led to an isotopic enrichment in water vapor, but the strong rainout effects caused an isotopic depletion in precipitation (Figs. 7c and 7d). The spatial distributions of Ex_d_v and Ex_d_p in June showed no significant differences compared to the situations in April (Figs. 5e, 5f, 7e, and 7f). The high-value regions for the Ex_d_v and Ex_d_p were located in the region stretching from western Asia through the Tibetan Plateau to southwestern China, as well as in the vast oceanic region centered around the Philippines and Indonesia. Under the influence of the summer monsoon, the difference in deuterium excess between East Asia and its water vapor source—that is, the low-latitude ocean, remained relatively small (Figs. 7e and 7f).

Based on the vector interpolation of the Q field (Fig. 7a), the water vapor transport path regarding the Dongting Lake Basin as the endpoint was determined in June (shown by the black arrow lines in Fig. 7). This water vapor transport path originated from the northern branch of the South Indian Ocean subtropical high, crossed the equator, and transported through the Somali Sea, the Arabian Sea, the Indian Peninsula, the Bay of Bengal, the Indochinese Peninsula, and entered the southwestern region of China, finally reaching the Dongting Lake Basin. It can be seen that this water vapor transport path was consistent with the prevailing wind direction in June as shown in Fig. 1a. The

https://doi.org/10.5194/egusphere-2024-2215
Preprint. Discussion started: 19 August 2024

corresponding Q, P, $\delta^{18}O_v$, $\delta^{18}O_p$, Ex_d_v, and Ex_d_p along the water vapor transport path were extracted, and plotted in Fig. 8.

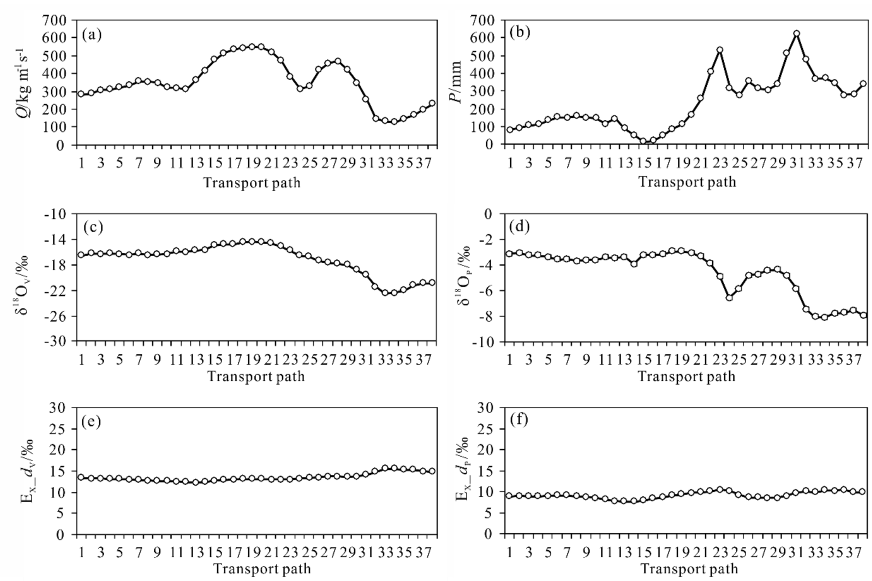

Fig. 8 Mean variations of Q (a), P (b), $\delta^{18}O_v$ (c), $\delta^{18}O_p$ (d), Ex_d_v (e), and Ex_d_p (f) along the vapor transport path in June.

Along the water vapor transport path, the average Q and P were at their maximum throughout the year, reaching 353.86 kg m^{-1} s^{-1} and 236.5 mm, respectively (Figs. 8a and 8b). The three extreme values of the Q along the transport path, or in the process of transitioning from the maximum to minimum values, correspond to three P extremes located at the western coast of the Indian Peninsula, the border region between Thailand and Myanmar, and the region around the Dongting Lake Basin (Fig. 7b), with the values of the three P extremes of 535.1 mm, 627.8 mm, and 341.5 mm, respectively (Fig. 8b). With continuous precipitation especially after experiencing heavy precipitation and the simultaneous persistent rainout processes, the stable isotopes in both water vapor and

https://doi.org/10.5194/egusphere-2024-2215
Preprint. Discussion started: 19 August 2024

precipitation exhibit a trend of continuous depletion (Figs. 8c and 8d). However, due to continuous water vapor supply from low-latitude oceans, there were no significant changes in both the Ex_d_v and Ex_d_p (Figs. 8e and 8f).

3.2.4 Average Water Vapor Transport Path in the Dongting Lake Basin in October

The spatial distributions of the average H_{500}, Q, P, $\delta^{18}Ov$, $\delta^{18}O_p$, Ex_d_v, and Ex_d_p in October were shown in Fig. 9. A notable feature at the H_{500} field in October was the expansion of the latitudinal westerlies toward lower latitudes (Fig. 9a). In East Asia, westerly winds prevail in the inland regions north of approximately 30°N, while much of the regions south of 30°N were still influenced by the subtropical high-pressure system. Compared to the peak period, the West Pacific subtropical high had significantly weakened in autumn, and its main body had also retreated to the open sea. However, a mesoscale anticyclone split from the high still controlled the Jiangnan region of China including the Dongting Lake Basin, creating a climate characterized by clear and crisp autumn (Fig. 9a). Due to the disappearance of the India-Burma Trough and influenced by the anticyclone circulation, the water vapor transport from the southwest low-latitude oceans decreased significantly. In the Dongting Lake Basin, both the meridional and latitudinal water vapor transport were even less than the values in January (Fig. 3a and 9a; Xiao et al., submitted). Apart from the autumn rains in western China, precipitation was generally scarce in East Asia in this period, with the rain belt shifting southward to lower latitudes corresponding to the convergence zone near the equator, with the largest precipitation regions located respectively south of the Equator in the Indian Ocean, the Malay Peninsula, and north of the Equator in the

https://doi.org/10.5194/egusphere-2024-2215
Preprint. Discussion started: 19 August 2024

western Pacific (Fig. 9b).

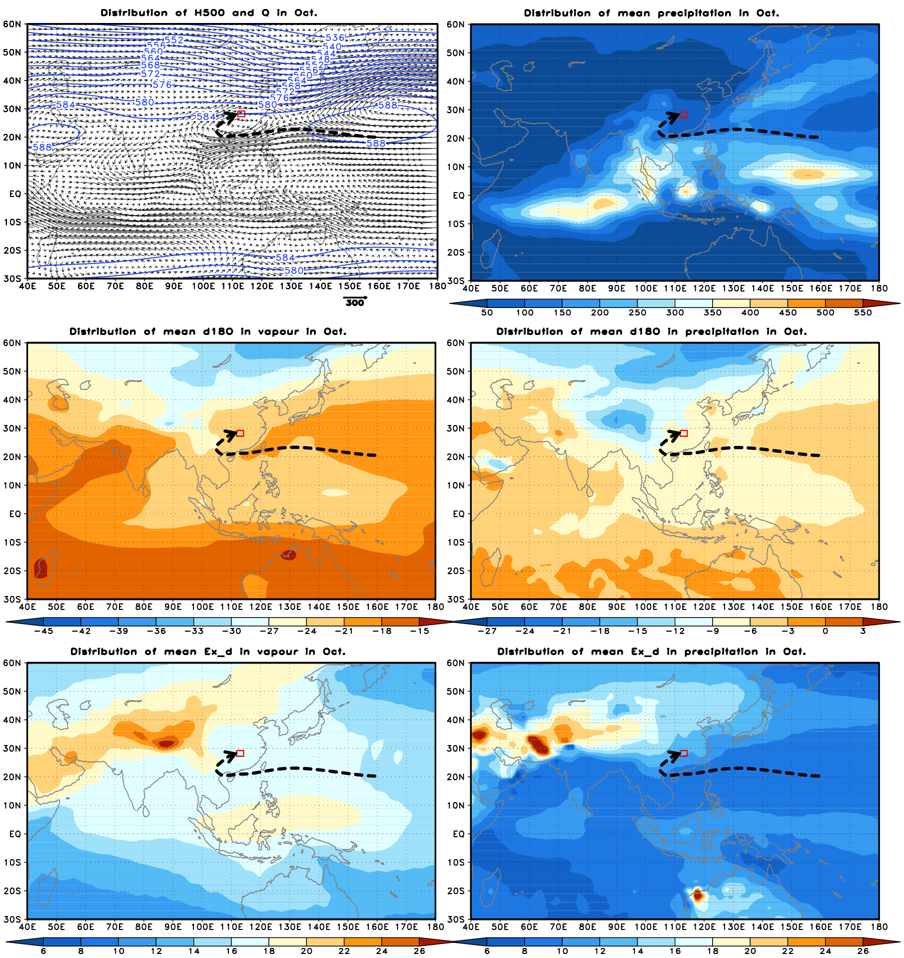

Fig. 9 Mean vapor transport path to the Dongting Lake Basin and the spatial distributions of Q with H_{500} (a), P (b), $\delta^{18}O_v$ (c), $\delta^{18}O_p$ (d), Ex_d_v (e), and Ex_d_p (f) in October.

Compared to the situations in June, there were no significant changes in the spatial distribution of the $\delta^{18}O_v$ and $\delta^{18}O_p$ in October, but their differences between land and sea as well as between high and low latitudes increased largely (Figs. 9c and 9d). The stable isotopes in water vapor and precipitation were significantly depleted in Eastern

https://doi.org/10.5194/egusphere-2024-2215
Preprint. Discussion started: 19 August 2024

Siberia and the Tibetan Plateau, and accompanied by expansion of ranges. As a result, the $\delta^{18}O_v$ and $\delta^{18}O_p$ showed a significant decrease in the inland regions north of approximately 30°N, but unchanging in most regions south of 30°N. From the spatial distributions in October, both the Ex_d_v and Ex_d_p over the ocean or on land showed increases with varying degrees (Figs. 9e and 9f). The high-value regions of the Ex_d_v were distributed along a line from the Arabian Peninsula, West Asia, the Tibetan Plateau, to Eastern Siberia, with the maximum value located in the Tibetan Plateau. The high-value region of Ex_d_p was distributed from the Arabian Peninsula, West Asia, the Tibetan Plateau, to the Yunnan-Guizhou Plateau. With the weakening of the summer monsoon, the Ex_d_v and Ex_d_p were not significantly different in East Asia including the Dongting Lake Basin from those in the surrounding oceans.

Based on the vector interpolation of the *Q* field (Fig. 9a), the water vapor transport path regarding the Changsha site as the endpoint was determined in October (indicated by the black arrow line in Fig. 9). This water vapor transport path originated from the western Pacific, passed through the South China Sea, flowed westward along the easterly jet located in the south of the West Pacific Subtropical High and of the anticyclonic circulation over the Jiangnan region in China, and finally entered the Dongting Lake Basin bypassing the southwest of the anticyclone. Although this water vapor path belonged to the latitudinal transport, the water vapor source originated from the low-latitude oceans of the western Pacific.

The corresponding *Q*, *P*, $\delta^{18}O_p$, $\delta^{18}O_v$, Ex_d_v, and Ex_d_p along the water vapor transport path were derived in October (Fig. 10). Under the stable atmospheric

https://doi.org/10.5194/egusphere-2024-2215
Preprint. Discussion started: 19 August 2024

circulation conditions, the average water vapor flux steadily decreased from approximately 299.0 kg m^{-1} s^{-1} in the source region to 168.0 kg m^{-1} s^{-1} along the water vapor transport path, and further below 100.0 kg m^{-1} s^{-1}after entering the Dongting Lake Basin (Fig. 10a). The *P* values changed gradually along the water vapor transport path, decreasing from the initial approximately 145 mm to below 100 mm in the Dongting Lake Basin, and further to 60.5 mm in the Changsha region (Fig. 10b). Both the $\delta^{18}O_v$ and $\delta^{18}O_p$ values showed slow decreases as the ranges within 2.0‰ and 1.0‰ respectively (Figs. 10c and 10d). The Ex_d_v showed minor fluctuation, stabilizing at approximately 16.8‰, while the corresponding Ex_d_p remained around 8.62‰ before entering the Dongting Lake Basin. Due to the replenishment from the surface evaporation, the Ex_d_p values increased to 11.60‰ after entering the Dongting Lake Basin (Figs. 10e and 10f).

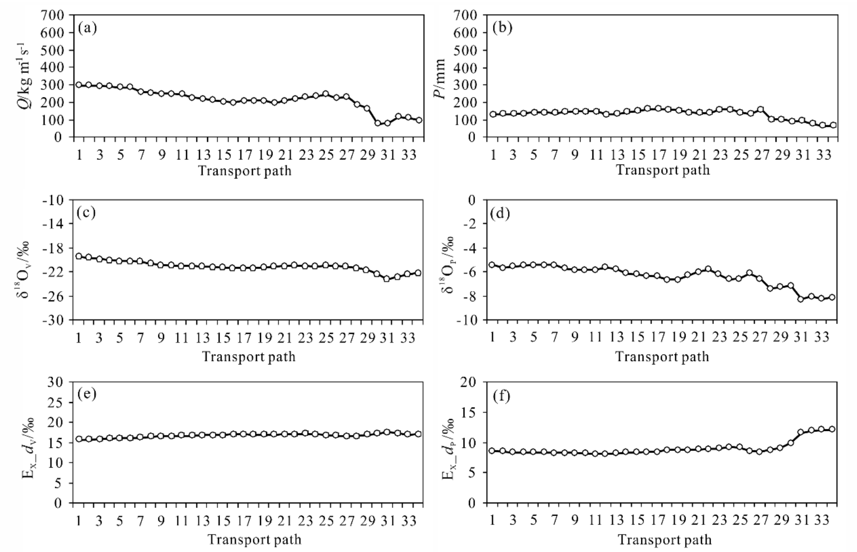

Fig. 10 Mean variations of *Q* (a), *P* (b), $\delta^{18}O_v$ (c), $\delta^{18}O_p$ (d), Ex_d_v (e), and Ex_d_p (f) along the vapor transport path in October

https://doi.org/10.5194/egusphere-2024-2215
Preprint. Discussion started: 19 August 2024

4. Discussion

4.1 The Influences of the Seasonality in Water Vapor Sources on the Precipitation Isotopes.

The comparisons between the *Q* and $\delta^{18}O_p$ in the representative months indicated that there seems to be no obvious correspondence between these two factors: the months with low *Q* would exhibit either high or low $\delta^{18}O_p$, e.g. January and October, respectively (Figs. 3 and 9). Similarly, the months with high *Q* would exhibit either low or high $\delta^{18}O_p$, for example, June and April, respectively (Figs. 5 and 7). It has been found that regardless of the season, the precipitation in the Dongting Lake Basin mainly originated from warm and moist water vapor in low latitudes (Figs. 3, 5, 7, and 9). Therefore, whether the water vapor isotopes at the source regions and along the transport path influence the downstream isotopes of precipitation or water vapor? To reveal this causality, after considering the water vapor transport paths and the air mass properties of water vapor in the representative months, the regions corresponding to the Arabian Peninsula (40°E~56°E, 16°N~28°N), the Arabian Sea (56°E~74°E, 10°N~20°N), the Bay of Bengal (80°E~98°E, 8°N~18°N), the western Pacific Ocean (120°E~160°E, 6°N~20°N), the Dongting Lake Basin (110°E~114°E, 25°N~30°N), and the inland regions of East Asia monsoon region (110°E~135°E, 42°N~55°N) were labeled as Regions I, II, III, IV, V, and VI, respectively (Fig. 11). The average $\delta^{18}O$ and Ex_d of water vapor and precipitation for each representative region were calculated in January, April, June, and October, respectively. Since the seasonal variations in the $\delta^{18}O_v$ were similar to that in $\delta^{18}O_p$, Table 1 only provided the average $\delta^{18}O$ and Ex_d

https://doi.org/10.5194/egusphere-2024-2215
Preprint. Discussion started: 19 August 2024

of water vapor for each representative region.

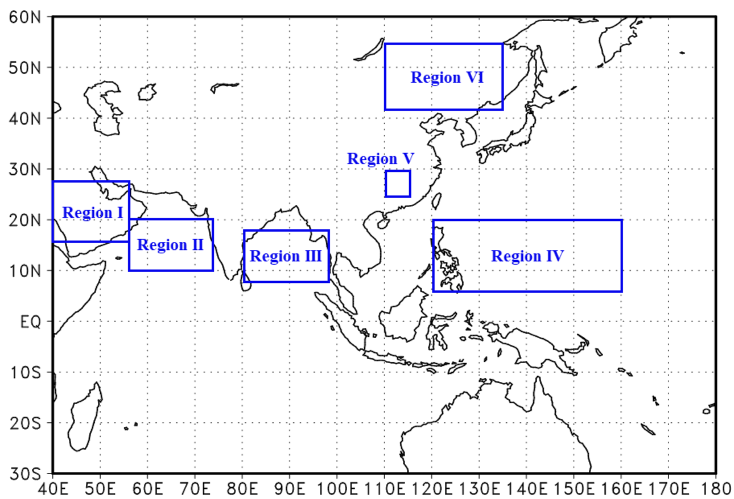

Fig. 11 Geographical distribution of representative regions

(Region I: Arabian Peninsula, Region II: Arabian Sea, Region III: Bay of Bengal, Region IV: Western Pacific, Region V: Dongting Lake Basin, Region VI: Inland of the East Asian monsoon region at middle and high latitudes)

Not only in Regions I to V located at mid to low latitudes but also in Region VI located in the mid to high latitude inland regions, there were significant seasonal variations in the average $\delta^{18}O_v$ and Ex_d_v (Table 1). The seasonal differences in the $\delta^{18}O_v$ (the differences between the monthly maximum and minimum values) in these six representative regions were 2.94‰, 3.34‰, 4.19‰, 5.06‰, 7.18‰, and 18.94‰, respectively, with the largest seasonal difference in $\delta^{18}O_v$ appeared in Region VI (Table 1). Except for Region VI, the minimum values of the monthly $\delta^{18}O_v$ in other representative regions, all occurred in October, while the maximum or second maximum values occurred in April. The seasonal differences in the Ex_d_v in these six

https://doi.org/10.5194/egusphere-2024-2215
Preprint. Discussion started: 19 August 2024

representative regions were 4.69‰, 5.42‰, 3.56‰, 3.81‰, 3.59‰, and 9.31‰, respectively, with the largest seasonal difference in the Ex_d_v still in Region VI. Except for Region VI, the maximum values of monthly Ex_d_v in other representative regions mostly occurred in October, while the minimum or second minimum values occurred in April or June (Table 1). These results indicated significant differences in water vapor isotopes between Region VI and other representative regions.

Table 1 Mean $\delta^{18}O_v$ and Ex_d_v for representative regions in the representative months

Factors	Months	Region I	Region II	Region III	Region IV	Region V	Region VI
$\delta^{18}O_v$ /‰	January	-19.04	-17.42	-18.72	-17.24	-18.82	-40.93
	April	-16.22	-15.78	-17.83	-17.94	-14.91	-28.70
	June	-17.10	-14.45	-18.10	-21.92	-20.77	-21.99
	October	-19.16	-17.79	-22.02	-22.30	-22.09	-29.32
Ex_d_v /‰	January	18.45	18.51	17.22	14.39	15.21	23.20
	April	16.93	17.46	17.03	13.91	13.55	15.64
	June	16.04	13.09	13.98	16.25	15.03	13.89
	October	20.73	17.33	17.54	17.72	17.14	18.29

According to the statistics in Table 1, in January, the average $\delta^{18}O_v$ and Ex_d_v were −19.04‰ and 18.45‰, respectively, in Region I under the latitudinal water vapor transport, while −18.82‰ and 15.21‰, respectively, in Region V with their differences only 0.22‰ and 3.24‰, respectively; In April, the average $\delta^{18}O_v$ and Ex_d_v were −16.22‰ and 16.93‰, respectively, in Region I also under the latitudinal water vapor transport, while −17.94‰ and 13.91‰, respectively, in Region IV under the meridional water vapor transport, and −14.91‰ and 13.55‰, respectively, in Region V; In June, the average $\delta^{18}O_v$ were −14.45‰ and −18.10‰, respectively, the average Ex_d_v values

https://doi.org/10.5194/egusphere-2024-2215
Preprint. Discussion started: 19 August 2024

were 13.09‰ and 13.98‰, respectively, in Regions II and III, all under the meridional water vapor transport, while the average $\delta^{18}O_v$ and average Ex_d$_v$ were −20.77‰ and 15.03‰, respectively, in Region V after experiencing intense rainout processes; In October, the average $\delta^{18}O_v$ and Ex_d$_v$ were −22.30‰ and 17.72‰, respectively, in Region IV under the weakened meridional water vapor transport, showing non-significantly differences from the values of −22.09‰ and 17.14‰, respectively, in Region V (Table 1).

Furtherly, by comparing the water vapor isotopes in Region V with those in Region VI, it can be found that although both regions were all located in the East Asian monsoon region, there were differences in the seasonal variations of water vapor isotopes (Table 1; Fig. 11). For instance, the average $\delta^{18}O_v$ in Regions V and VI in all of the representative months were −19.15‰ and −30.24‰, respectively, with a difference of 11.09‰. Moreover, the average $\delta^{18}O_v$ of these two regions showed the largest differences with a value of 22.11‰ in January, which represented the peak of the winter monsoon, while in June which represented the peak of the summer monsoon, the difference was only 1.22‰. The water vapor isotopes in Region V were consistently enriched compared to those in Region VI. The average Ex_d$_v$ in Regions V and VI in all of the representative months were 15.23‰ and 17.76‰, respectively, with a difference of −2.52‰, which was not too large. The difference was largest in January, reaching −7.99‰, while in June, the difference was only 1.14‰, indicating that the water vapor sources during the summer monsoon were similar in these two regions (Table 1).

https://doi.org/10.5194/egusphere-2024-2215
Preprint. Discussion started: 19 August 2024

The above results about the water stable isotope differences between the representative regions conform to the latitudinal and continental effects of water stable isotopes and follow the law of material migration, which states that the composition of water stable isotopes becomes more depleted with increasing latitude and water vapor transport from high to low value regions (Feng et al., 2009; Zhang et al., 2012; Zhang et al., 2016). With emphasis, for the water vapor source of precipitation in the Dongting Lake Basin, the oceanic representative regions located at low latitudes may not necessarily be the initial water vapor source regions, and the relationship between upstream and downstream regions may not entirely be point-to-point, as there were continuous water recycling and rainout processes along the water vapor transport path (Pokam et al., 2012; Risi et al., 2013; Christner et al., 2018). However, through the comparisons above, it can be observed that the influences of upstream regions on the water vapor amount and water vapor isotopes in downstream regions during water vapor transport were significant.

4.2 Isotopic Properties of Air Masses

According to the definition of meteorology, air mass refers to a large-scale body of air over land or sea with relatively uniform horizontal physical properties such as temperature, humidity, and atmospheric stability. The horizontal extent of an air mass ranges from 10^2 km to 10^3 km, and the vertical extent ranges from 10^0 km to 10^1 km, while within the same air mass, there is little variation in temperature gradients, atmospheric vertical stability, and weather phenomena (Zhou et al., 1997). Under large-scale and relatively uniform underlying surfaces and stable atmospheric circulation

https://doi.org/10.5194/egusphere-2024-2215
Preprint. Discussion started: 19 August 2024

conditions, water vapor and its transport belong to the characteristics of air masses or have the properties of the air mass origin regions (Dettinger, 2013; Lavers et al., 2013). Considering the sources and sinks of water vapor, the spatial distribution of water vapor isotopes is relatively similar within an air mass. In maritime air masses, water vapor isotopes are relatively enriched, while deuterium excess of water vapor is relatively more negative, while in continental air masses, water vapor isotopes are relatively depleted, while excess deuterium of water vapor is relatively more negative (Rozanski et al., 1993; Araguás-Araguás et al., 1998).

With the seasonal variation in the position of the sun's orbit, the atmospheric circulation conditions undergo seasonal variations and thus lead to the seasonality of the air masses properties (Qian et al., 2009; Parding et al., 2016). The abundance of water vapor isotopes at a fixed location varies due to variations in circulation conditions (Lacour et al., 2018; Dee et al., 2018; Gou et al., 2022). In this study, the isotopic compositions of water vapor in maritime Regions II and IV at low latitudes and in inland Region VI at high latitudes exhibited significant seasonal variations due to interactions between tropical continental air masses (located in southern West Asia) and tropical maritime air masses, between tropical maritime air masses and equatorial air masses, and between temperate continental air masses and temperate maritime air masses, respectively (Table 1; Fig. 11). In the process of seasonal changes, as air masses move out of their source regions, their physical and weather characteristics also change with the variations in underlying surface properties and large-scale vertical motion conditions. East Asia is primarily controlled by modificatory air masses (Ding, 1990;

https://doi.org/10.5194/egusphere-2024-2215
Preprint. Discussion started: 19 August 2024

Chang et al., 2012). Whether cold and dry air masses moving southward or warm and moist air masses moving northward, the isotopic composition of water vapor in the modificatory air mass continues to become more negative, while the deuterium excess of water vapor continues to become more positive than the original air mass (Zhou et al., 2019; Xu et al., 2019; Jackisch et al., 2022). In this study, interactions between modificatory marine air mass and modificatory continental air mass result in the water vapor isotope in Region V that differed from maritime air masses and continental air masses (Table 1; Fig. 11). In summary, as an important member of the climate system, air mass possesses not only thermodynamic, dynamic, hydrous and static properties but also isotopic properties.

4.3 The Difference Between Water Vapor Field and Wind Field

The water vapor flux Q reflects the direction and magnitude of water vapor transport in the atmosphere, while wind V reflects the direction and magnitude of the movement of air particles in the atmosphere (Feng et al., 2009; Zhang et al., 2012; Zhang et al., 2016). There are both differences and connections between the two factors. Water vapor is transported by wind, and the wind carries water vapor from one place to another, and the directions of water vapor and wind may be consistent, inconsistent, or even opposite. In the East Asian monsoon region, the prevailing wind direction during the summer monsoon period is generally consistent with the average water vapor transport direction, both being southwest or southeast direction (Barker, et al., 2015; Wu et al., 2015; Tang et al., 2015). In this study, the water vapor transport path was consistent with the prevailing wind direction in June (Figs. 1a and 9). However, during

https://doi.org/10.5194/egusphere-2024-2215
Preprint. Discussion started: 19 August 2024

the winter monsoon period, the prevailing wind direction may not be consistent with the average transport direction of water vapor—that is, the prevailing wind direction in January was northwest or northeast direction, while the average transport direction of water vapor in this period was southwest or southeast direction (Figs. 1a and 3), and supported by the water vapor transport study focusing on the Changsha region (Xiao et al., submitted).

Previous studies have shown that the most common weather systems and most precipitation events in the East Asian monsoon region are caused by cold fronts resulting from the interaction of warm and cold air masses (Chen et al., 2020). According to classical meteorological theory (Zhou et al., 1997), in a cold front system, there appears the wind from the southwest direction blows ahead of the front, and a northwest wind blows behind the front as shown in the schematic diagram in Fig. 12a. Warm and moist air from low latitudes lifts along the front and leads to rainfall, while cold and dry air from high latitudes moves southward beneath the front and lifts the warm and moist air. At different altitudes and positions, the directions of air particle movement and water vapor transport are different. For example, at the point A located above the warm and moist air side of the cold front surface, both air particles and water vapor are transported by southwest wind. At the point C located below the cold, dry air side of the cold front surface, both air particles and water vapor are transported by northwest wind. However, at the point B located within the front zone, the wind direction and speed are uncertain (Fig. 12b). Therefore, the dominant wind directions may not always align with the average water vapor transport direction, especially in

https://doi.org/10.5194/egusphere-2024-2215
Preprint. Discussion started: 19 August 2024

frontal weather systems that dominate precipitation in the East Asian monsoon region.

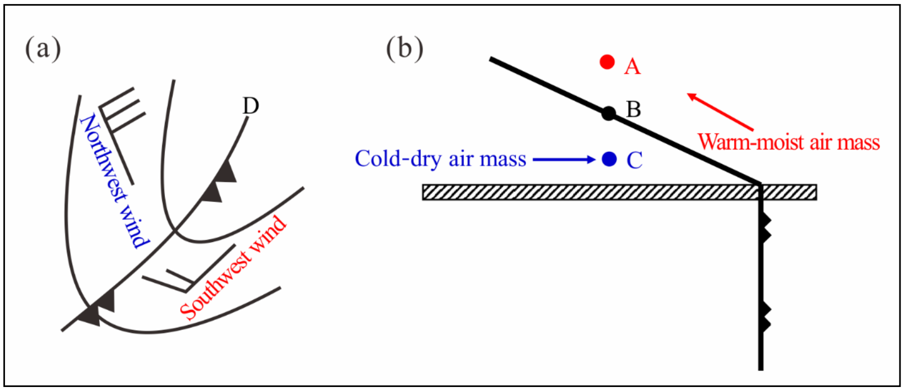

Fig. 12 Schematic diagram of a cold front system in East Asia (based on Zhou et al., 1997).

4. Conclusion

Our findings revealed significant influences of water vapor source and transport on precipitation isotopes in Dongting Lake Basin. Specifically, in January, water vapor contributing to the Dongting precipitation originated near the Arabian Peninsula and was driven by the southern branch of the westerly stream jet on the southern side of the Tibetan Plateau, water vapor transported along the southern side of the Tibetan Plateau, passed through southwestern China via the northern part of the Indian Peninsula, and reached the Dongting Lake Basin. In April, two distinct water vapor transport paths contributed to the Dongting precipitation, the first followed a trajectory similar to the average water vapor transport path in January, albeit shifted slightly northward by one degree of latitude. The second transport path, driven by the weak Western Pacific subtropical high, guided warm and moist water vapor from the low latitudes of the Western Pacific along the outer edge of the subtropical high, passing through the South

https://doi.org/10.5194/egusphere-2024-2215
Preprint. Discussion started: 19 August 2024

China Sea and the Indochinese Peninsula and finally reached into the Dongting Lake Basin. In June, the Dongting precipitation was influenced by a water vapor transport path originating from the northern branch of the South Indian Ocean subtropical high, crossed the equator, and transported through the Somali Sea, the Arabian Sea, the Indian Peninsula, the Bay of Bengal, the Indochinese Peninsula, and entered the southwestern region of China, finally reaching the Dongting Lake Basin. In October, the average water vapor transport path originated from the western Pacific, passed through the South China Sea, flowed westward along the easterly jet located in the south of the West Pacific Subtropical High and of the anticyclonic circulation over the Jiangnan region in China, and finally entered the Dongting Lake Basin bypassing the southwest of the anticyclone. Although this water vapor path belonged to the latitudinal transport, the water vapor source originated from the low-latitude oceans of the western Pacific. In these four months that representing different seasons, variations in the $\delta^{18}O$ and Ex_d of precipitation and water vapor along these water vapor transport paths adhered to principles of Rayleigh fractionation and water balance principles, underscoring the complex transport paths and processes that influence isotopic variations in precipitation in the Dongting Lake Basin. However, the prevailing wind direction may not be consistent with the average transport direction of water vapor, especially during the winter monsoon, which can be explained by the water vapor field and wind field in frontal weather systems that dominate precipitation in the East Asian monsoon region.

Overall, the approach utilized in this study is grounded in fundamental meteorological theories, specifically involving water vapor diagnosis and calculations

https://doi.org/10.5194/egusphere-2024-2215
Preprint. Discussion started: 19 August 2024

(including source regions, transport paths, and transport quantities), this analytical method is robust and has a clear physical basis. The scientific question addressed by this study is not centered on the spatial and temporal variations of water isotopes, but rather on how the seasonal variations in regional precipitation and precipitation isotopes respond to the seasonal variations in water vapor sources and transport.

Competing interests

The authors declare that they have no known competing financial interests or personal relationships that could have appeared to influence the work reported in this paper.

Acknowledgments

This study was supported by the Natural Science Foundation of Hunan Province, China (No. 2023JJ40445) the National Natural Science Foundation of China (No. 42101130), and the Aid Program for Science and Technology Innovative Research Team in Higher Educational Institutions of Hunan Province (0531120-4944). We are grateful to the graduate students who laboriously sampled water samples without interruption and tested water stable isotopes for 13 years.

Author contribution

Xiong Xiao: Methodology, Software, Writing- Original draft preparation, Reviewing and Editing. Xinping Zhang: Supervisor, Guide, Data curation, Methodology, Software, Writing- Original draft preparation, Reviewing and Editing. Zhuoyong Xiao: Methodology, Writing-Original draft preparation. Zhongli Liu, Dizhou Wang, Cicheng Zhang, Zhiguo Rao, Xinguang He, and Huade Guan: Methodology, Reviewing and Editing. All authors made substantial contributions to the discussion of content.

https://doi.org/10.5194/egusphere-2024-2215
Preprint. Discussion started: 19 August 2024

Code/Data availability

The global atmospheric reanalysis data and water stable isotope simulation data are downloaded from the ECMWF 5th generation atmospheric reanalysis data (ERA5, https://cds.climate.copernicus.eu/) and the second-generation isoGSM2 dataset (https://datadryad.org/stash/dataset/doi:10.6078/D1MM6B), respectively. The stable isotopic data of precipitation and meteorological data at the Changsha station are accessible by emailing the corresponding author (zxp@hunnu.edu.cn) with a reasonable request.

References:

Albergel, C., Dutra, E., Munier, S., Calvet, J. C., Munoz-Sabater, J., de Rosnay, P., & Balsamo, G. (2018). ERA-5 and ERA-Interim driven ISBA land surface model simulations: which one performs better?. Hydrology and Earth System Sciences, 22(6), 3515-3532.

Araguás-Araguás, L., Froehlich, K., & Rozanski, K. (1998). Stable isotope composition of precipitation over southeast Asia. Journal of Geophysical Research: Atmospheres, 103(D22), 28721-28742.

Baker, A. J., Sodemann, H., Baldini, J. U., Breitenbach, S. F., Johnson, K. R., van Hunen, J., & Zhang, P. (2015). Seasonality of westerly moisture transport in the East Asian summer monsoon and its implications for interpreting precipitation $\delta^{18}O$. Journal of Geophysical Research: Atmospheres, 120(12), 5850-5862.

Bong, H., Cauquoin, A., Okazaki, A., Chang, E. C., Werner, M., Wei, Z., ... & Yoshimura, K. (2024). Process-Based Intercomparison of Water Isotope-Enabled

https://doi.org/10.5194/egusphere-2024-2215
Preprint. Discussion started: 19 August 2024

Models and Reanalysis Nudging Effects. Journal of Geophysical Research: Atmospheres, 129(1), 1-28.

Chang, C. P., Lei, Y., Sui, C. H., Lin, X., & Ren, F. (2012). Tropical cyclone and extreme rainfall trends in East Asian summer monsoon since mid-20th century. Geophysical Research Letters, 39(18), 1-7.

Chen, X., Zhang, X. Z., Zhang X. P., & Long X. (2020). Long-term Variation of Regional Extreme Precipitation in jiangnan Area and lts Possible Cause. Resources and Environment in The Yangtze Basin, 29(08),1757-1767.

Chiang, J. C., Herman, M. J., Yoshimura, K., & Fung, I. Y. (2020). Enriched East Asian oxygen isotope of precipitation indicates reduced summer seasonality in regional climate and westerlies. Proceedings of the National Academy of Sciences, 117(26), 14745-14750.

Christner, E., Aemisegger, F., Pfahl, S., Werner, M., Cauquoin, A., Schneider, M., ... & Schädler, G. (2018). The climatological impacts of continental surface evaporation, rainout, and subcloud processes on δD of water vapor and precipitation in Europe. Journal of Geophysical Research: Atmospheres, 123(8), 4390-4409.

Dahinden, F., Aemisegger, F., Wernli, H., Schneider, M., Diekmann, C. J., Ertl, B., ... & Pfahl, S. (2021). Disentangling different moisture transport pathways over the eastern subtropical North Atlantic using multi-platform isotope observations and high-resolution numerical modelling. Atmospheric Chemistry and Physics, 21(21), 16319-16347.

Dee, S. G., Nusbaumer, J., Bailey, A., Russell, J. M., Lee, J. E., Konecky, B., ... & Noone, D. C. (2018). Tracking the strength of the Walker circulation with stable isotopes in water vapor. Journal of Geophysical Research: Atmospheres, 123(14), 7254-7270.

Deng, H., Wang, Q., Zhao, Y., Zhai, J., Zhu, Y., Gui, Y., ... & Liu, K. (2024). Effect of water vapor transport and budget on precipitation in the Yangtze–Huang–Huai–Hai River Basin. Journal of Hydrology: Regional Studies, 53, 101787.

Dettinger, M. D. (2013). Atmospheric rivers as drought busters on the US West Coast. Journal of Hydrometeorology, 14(6), 1721-1732.

Ding, Y., 1990: Build-up, air mass transformation and propagation of Siberian high and its relations to cold surge in East Asia. Meteorology and Atmospheric Physics, 44, 281–292.

Esquivel-Hernández, G., Mosquera, G. M., Sánchez-Murillo, R., Quesada-Román, A., Birkel, C., Crespo, P., ... & Boll, J. (2019). Moisture transport and seasonal variations in the stable isotopic composition of rainfall in Central American and Andean Páramo during El Niño conditions (2015–2016). Hydrological Processes, 33(13), 1802-1817.

Feng, X., Faiia, A. M., & Posmentier, E. S. (2009). Seasonality of isotopes in precipitation: A global perspective. Journal of Geophysical Research: Atmospheres, 114(D8), 1-13.

https://doi.org/10.5194/egusphere-2024-2215
Preprint. Discussion started: 19 August 2024

Gimeno, L., Vázquez, M., Eiras-Barca, J., Sorí, R., Stojanovic, M., Algarra, I., ... & Dominguez, F. (2020). Recent progress on the sources of continental precipitation as revealed by moisture transport analysis. Earth-Science Reviews, 201, 103070.

Gou, J., Qu, S., Guan, H., Shi, P., Su, Z., Lin, Z., ... & Zhu, J. (2022). Relationship between precipitation isotopic compositions and synoptic atmospheric circulation patterns in the lower reach of the Yangtze River. Journal of Hydrology, 605, 127289, 1-15.

Guo, L., Van Der Ent, R. J., Klingaman, N. P., Demory, M. E., Vidale, P. L., Turner, A. G., ... & Chevuturi, A. (2019). Moisture sources for East Asian precipitation: Mean seasonal cycle and interannual variability. Journal of Hydrometeorology, 20(4), 657-672.

He, H., Cao, R., Wu, Z. Y., Li, Y., Yin, H., & Yuan, F. (2022). Diagnosing anomalous characteristics of atmospheric water cycle structure during seasonal-scale drought events: A case study in middle and lower reaches of Yangtze River. Water Science and Engineering, 15(2), 103-113.

Hoffmann, L., Günther, G., Li, D., Stein, O., Wu, X., Griessbach, S., ... & Wright, J. S. (2019). From ERA-Interim to ERA5: the considerable impact of ECMWF's next-generation reanalysis on Lagrangian transport simulations. Atmospheric Chemistry and Physics, 19(5), 3097-3124.

Hu, Q., Jiang, D., Lang, X., & Yao, S. (2021). Moisture sources of summer precipitation over eastern China during 1979–2009: A Lagrangian transient simulation. International Journal of Climatology, 41(2), 1162-1178.

https://doi.org/10.5194/egusphere-2024-2215
Preprint. Discussion started: 19 August 2024

Huang, H., & Li, L. (2023). A Synchronous Variation Process of Tibetan Plateau Vortex and Southwest Vortex (in Chinese). Journal of Applied Meteorological Science, 34(4), 451-462.

Jackisch, D., Yeo, B. X., Switzer, A. D., He, S., Cantarero, D. L. M., Siringan, F. P., & Goodkin, N. F. (2022). Precipitation stable isotopic signatures of tropical cyclones in Metropolitan Manila, Philippines, show significant negative isotopic excursions. Natural Hazards and Earth System Sciences, 22(1), 213-226.

Kathayat, G., Sinha, A., Tanoue, M., Yoshimura, K., Li, H., Zhang, H., & Cheng, H. (2021). Interannual oxygen isotope variability in Indian summer monsoon precipitation reflects changes in moisture sources. Communications Earth & Environment, 2(1), 1-10.

Lacour, J. L., Risi, C., Worden, J., Clerbaux, C., & Coheur, P. F. (2018). Importance of depth and intensity of convection on the isotopic composition of water vapor as seen from IASI and TES δD observations. Earth and Planetary Science Letters, 481, 387-394.

Lai, X., Wang, Q., Huangfu, J., Jiang, X., Wang, L., Chen, W., ... & Tang, Yu. (2023). Progress in Climatological Research on the Southwest China Vortex (in Chinese). Chinese Journal of Atmospheric Sciences, 47(6), 1983-2000.

Lavers, D. A., Allan, R. P., Villarini, G., Lloyd-Hughes, B., Brayshaw, D. J., & Wade, A. J. (2013). Future changes in atmospheric rivers and their implications for winter flooding in Britain. Environmental Research Letters, 8(3), 034010, 1-8.

https://doi.org/10.5194/egusphere-2024-2215
Preprint. Discussion started: 19 August 2024

Lekshmy, P. R., Midhun, M., & Ramesh, R. (2022). Role of moisture transport from Western Pacific region on water vapor isotopes over the Bay of Bengal. Atmospheric Research, 265, 105895.

Liang, Y., Zhao, K., Edwards, R. L., Wang, Y., Shao, Q., Zhang, Z., ... & Kong, X. (2020). East Asian monsoon changes early in the last deglaciation and insights into the interpretation of oxygen isotope changes in the Chinese stalagmite record. Quaternary Science Reviews, 250, 106699, 1-5.

Liu, J., Song, X., Fu, G., Liu, X., Zhang, Y., & Han, D. (2011). Precipitation isotope characteristics and climatic controls at a continental and an island site in Northeast Asia. Climate Research, 49(1), 29-44.

Liu, X., Yang, M., Wang, H., Liu, K., Dong, N., Wang, H., ... & Fan, W. (2023). Moisture sources and atmospheric circulation associated with the record-breaking rainstorm over Zhengzhou city in July 2021. Natural Hazards, 116(1), 817-836.

Liu, Z., Zhang, X., Xiao, Z., He, X., Rao, Z., & Guan, H. (2022). The relationships between summer droughts/floods and oxygen stable isotope composition of precipitation in Dongting Lake Basin. Quaternary Science, 42(2), 472-486.

Nie, Y., & Sun, J. (2022). Moisture sources and transport for extreme precipitation over Henan in July 2021. Geophysical Research Letters, 49(4), 1-10.

Parding, K., Olseth, J. A., Liepert, B. G., & Dagestad, K. F. (2016). Influence of atmospheric circulation patterns on local cloud and solar variability in Bergen, Norway. Theoretical and Applied Climatology, 125, 625-639.

https://doi.org/10.5194/egusphere-2024-2215
Preprint. Discussion started: 19 August 2024

Pérez-Alarcón, A., Fernández-Alvarez, J. C., Sorí, R., Nieto, R., & Gimeno, L. (2023). Moisture source identification for precipitation associated with tropical cyclone development over the Indian Ocean: a Lagrangian approach. Climate Dynamics, 60(9), 2735-2758.

Pokam, W. M., Djiotang, L. A. T., & Mkankam, F. K. (2012). Atmospheric water vapor transport and recycling in Equatorial Central Africa through NCEP/NCAR reanalysis data. Climate Dynamics, 38, 1715-1729.

Pranindita, A., Wang-Erlandsson, L., Fetzer, I., & Teuling, A. J. (2022). Moisture recycling and the potential role of forests as moisture source during European heatwaves. Climate Dynamics, 58(1), 609-624.

Qian, L., Solomon, S. C., & Kane, T. J. (2009). Seasonal variation of thermospheric density and composition. Journal of Geophysical Research: Space Physics, 114(A1), 1-15.

Rao, Z., Chen, F., Cheng, H., Liu, W., Wang, G. A., Lai, Z., & Bloemendal, J. (2013). High-resolution summer precipitation variations in the western Chinese Loess Plateau during the last glacial. Scientific Reports, 3(1), 2785, 1-6.

Rao, Z., Jia, G., Li, Y., Chen, J., Xu, Q., & Chen, F. (2016). Asynchronous evolution of the isotopic composition and amount of precipitation in north China during the Holocene revealed by a record of compound-specific carbon and hydrogen isotopes of long-chain n-alkanes from an alpine lake. Earth and Planetary Science Letters, 446, 68-76.

Risi, C., Bony, S., Vimeux, F., Frankenberg, C., Noone, D., & Worden, J. (2010). Understanding the Sahelian water budget through the isotopic composition of water vapor and precipitation. Journal of Geophysical Research: Atmospheres, 115(D24), 1-23.

Risi, C., Noone, D., Frankenberg, C., & Worden, J. (2013). Role of continental recycling in intraseasonal variations of continental moisture as deduced from model simulations and water vapor isotopic measurements. Water Resources Research, 49(7), 4136-4156.

Rozanski, K., Araguás-Araguás, L., & Gonfiantini, R. (1993). Isotopic patterns in modern global precipitation. Climate change in continental isotopic records, 78, 1-36.

Sengupta, S., & Sarkar, A. (2006). Stable isotope evidence of dual (Arabian Sea and Bay of Bengal) vapour sources in monsoonal precipitation over north India. Earth and Planetary Science Letters, 250(3-4), 511-521.

Shi, Y., Jin, Z., Wu, A., Li, G., & Li, F. (2021). Stable isotopic characteristics of precipitation related to the environmental controlling factors in Ningbo, East China. Environmental Science and Pollution Research, 28, 10696-10706.

Sun, B., Zhu, Y., & Wang, H. (2011). The recent interdecadal and interannual variation of water vapor transport over eastern China. Advances in Atmospheric Sciences, 28, 1039-1048.

Tang, Y., Pang, H., Zhang, W., Li, Y., Wu, S., & Hou, S. (2015). Effects of changes in moisture source and the upstream rainout on stable isotopes in precipitation–a case

https://doi.org/10.5194/egusphere-2024-2215
Preprint. Discussion started: 19 August 2024

study in Nanjing, eastern China. Hydrology and Earth System Sciences, 19(10), 4293-4306.

Vasil'chuk, Y. K. (2014). New data on the tendency and causes of deuterium excess variations during one snowfall. Doklady Earth Sciences 459(1), 1400-1403.

Wei, Z., Lee, X., Liu, Z., Seeboonruang, U., Koike, M., & Yoshimura, K. (2018). Influences of large-scale convection and moisture source on monthly precipitation isotope ratios observed in Thailand, Southeast Asia. Earth and Planetary Science Letters, 488, 181-192.

Wu, H., Fu, C., Zhang, C., Zhang, J., Wei, Z., & Zhang, X. (2022). Temporal variations of stable isotopes in precipitation from Yungui Plateau: insights from moisture source and rainout effect. Journal of Hydrometeorology, 23(1), 39-51.

Wu, H., Zhang, X., Xiaoyan, L., Li, G., & Huang, Y. (2015). Seasonal variations of deuterium and oxygen-18 isotopes and their response to moisture source for precipitation events in the subtropical monsoon region. Hydrological Processes, 29(1), 90-102.

Xiao, Z., Zhang, X., Xiao, X., Chang, X., & He, X. (2024). The Effect of Convective/Advective Precipitation Partitions on the Precipitation Isotopes in the Monsoon Regions of China: A Case Study of Changsha. Journal of Hydrometeorology, 23(84), 581-590.

Xu, K., Zhong, L., Ma, Y., Zou, M., & Huang, Z. (2020). A study on the water vapor transport trend and water vapor source of the Tibetan Plateau. Theoretical and Applied Climatology, 140, 1031-1042.

https://doi.org/10.5194/egusphere-2024-2215
Preprint. Discussion started: 19 August 2024

Xu, T., Sun, X., Hong, H., Wang, X., Cui, M., Lei, G., ... & Jiang, X. (2019). Stable isotope ratios of typhoon rains in Fuzhou, Southeast China, during 2013–2017. Journal of Hydrology, 570, 445-453.

Yoshimura, K., Kanamitsu, M., Noone, D., & Oki, T. (2008). Historical isotope simulation using reanalysis atmospheric data. Journal of Geophysical Research: Atmospheres, 113(D19), 1-15.

Zhan, Z., Pang, H., Wu, S., Liu, Z., Zhang, W., Xu, T., ... & Hou, S. (2023). Determining key upstream convection and rainout zones affecting $\delta^{18}O$ in water vapor and precipitation based on 10-year continuous observations in the East Asian Monsoon region. Earth and Planetary Science Letters, 601, 117912.

Zhang, H., Cheng, H., Cai, Y., Spötl, C., Sinha, A., Kathayat, G., & Li, H. (2020). Effect of precipitation seasonality on annual oxygen isotopic composition in the area of spring persistent rain in southeastern China and its paleoclimatic implication. Climate of the Past, 16(1), 211-225.

Zhang, X., Guan, H., Zhang, X., He, X., Zhang, W., Wang, X., & Yao, T. (2016). Comparisons and assessment on stable isotopic effects in precipitation simulated by different models. Quaternary Sciences, 36(6), 1343-1357.

Zhang, X., Sun, Z., Guan, H., Zhang, X., Wu, H., & Huang, Y. (2012). GCM simulations of stable isotopes in the water cycle in comparison with GNIP observations over East Asia. Acta Meteorologica Sinica, 26(4), 420-437.

Zhou, H., Zhang, X., Yao, T., Hua, M., Wang, X., Rao, Z., & He, X. (2019). Variation of $\delta^{18}O$ in precipitation and its response to upstream atmospheric convection and

https://doi.org/10.5194/egusphere-2024-2215
Preprint. Discussion started: 19 August 2024

rainout: A case study of Changsha station, south-central China. Science of the total environment, 659, 1199-1208.

Zhou, S. Z. (1997). Meteorology and Climatology. Higher Education Press, Beijing, 118-222.